



## **Computational study of elastic buckling and post-buckling strength of steel decks in bending**

Vitaliy V. Degtyarev<sup>1</sup>

### **Abstract**

The elastic buckling and post-buckling strength of steel decks in bending are examined computationally via finite element modeling. Nonlinear finite element models of steel deck were created in ANSYS and successfully validated against published experimental results. A parametric study comprising 472 simulations was conducted using the developed models to examine the influence of the deck cross-sectional geometry and thickness, boundary conditions, and transverse ties on the deck elastic buckling and post-buckling strength. The influence of the deck yield stress and steel constitutive models on the deck flexural strength was also investigated. The obtained local and distortional elastic buckling moments, as well as the ultimate moments for decks failing in local and distortional buckling, are discussed. It was found, in particular, that the post-buckling flexural strength of deck with flat compression flanges failing in local buckling is highly affected by the level of deck non-symmetry, in addition to the deck compression flange slenderness. The deck ultimate moments obtained in the parametric study are compared with those predicted by the AISI S100-16 direct strength and effective width methods. Design equations are proposed for predicting local elastic buckling coefficients of deck with flat compression flanges and distortional buckling coefficients of deck with intermediate stiffeners in compression flanges. Modifications of the direct strength method are proposed for better predictions of the flexural strength of deck with flat compression flanges failing in local and distortional buckling. The proposed equation predictions agree well with the numerical simulation results.

### **1. Introduction**

The Direct Strength Method (DSM) has been developed during the last twenty years (Schafer 2019) and is currently adopted in the North American Specifications for the Design of Cold-Formed Steel Structural Members (AISI S100-16) and in the Australian/New Zealand Standard for the design of cold-formed steel structures (AS/NZS 4600:2018). In contrast to the traditional Effective Width Method (EWM), DSM considers interaction of the member cross-section elements, such as webs and flanges. DSM offers advantages, especially for members that have their strength governed by distortional buckling and members with cross-sections optimized by longitudinal stiffeners of different shapes and sizes in webs and flanges (Schafer 2008).

---

<sup>1</sup> Design and Research Engineer, New Millennium Building Systems, <vitaliy.degtyarev@newmill.com>, <vitdegtyarev@yahoo.com>

Being an efficient method for many modern optimized sections, DSM was shown to be overly conservative for cross-sections with a very slender element in compression, such as steel deck and hat sections (Schafer and Peköz 1998, Schafer 2008). As the element slenderness increases, the elastic critical buckling stress of the slender element and the entire member decreases. DSM assumes that the ultimate strength of the entire member decreases with a decrease in the elastic critical buckling stress of the member. EWM, in contrast, assumes that the slender element only, not the entire section, has a reduced strength (Schafer 2008).

The DSM expression for local buckling of flexural members in AISI S100-16 was selected based on the analysis of a relatively large experimental database (Schafer and Peköz 1998), which in particular included flexural test results of trapezoidal decks without and with longitudinal intermediate stiffeners reported by Höglund (1980) and Bernard, Bridge, and Hancock (1993). The profiles with flat compression flanges in the database had the ratios of tension flange width to compression flange width of approximately 0.6 and 1.8 and the ratios of deck height to compression flange width of 0.8 and 0.6.

The experimental database also comprised hat sections without and with longitudinal intermediate stiffeners, including Winter test specimens of hat sections with a very slender compression flange and relatively narrow unstiffened tension flanges (Schafer and Peköz 1998). The DSM formula of AISI S100-16 considerably underestimated the moment capacity of those specimens. Schafer and Peköz (1998) reported that DSM conservatively predicted moment capacities of specimens with low ratios of height to compression flange width and tension flange width to compression flange width. Increases in the above-mentioned ratios resulted in less conservative predictions of the moment capacities. Overly conservative strength predictions were not observed for the deck sections with flat compression flanges probably because the above-mentioned ratios of the decks in the experimental database were not low enough to result in considerable discrepancies between the tests and the calculations.

The DSM expression for distortional buckling of flexural members in AISI S100-16 showed a good agreement with test results for trapezoidal decks with longitudinal intermediate stiffeners in the compression flanges that exhibited distortional buckling prior to failure (Bernard, Bridge, and Hancock 1993).

The literature review revealed very limited information about the elastic buckling and post-buckling strength of cold-formed steel (CFS) deck profiles in bending, especially the deck profiles commonly used in the US. As was previously mentioned, the DSM design provisions in AISI S100-16 were calibrated using results of physical tests conducted on European and Australian deck profiles, which are different from the US profiles. Recent studies on applicability of DSM to the US steel deck profiles confirmed that DSM underestimates moment capacity of decks with slender flat compression flanges (Dudenbostel and Sputo 2016, Raebel and Gwozdz 2018).

Finite element (FE) simulations of elastic buckling and collapse behavior of CFS steel members may be a good and efficient alternative to expensive and time consuming physical testing when FE models used in the simulations were appropriately built, calibrated, and validated using available test results (Schafer, Li, and Moen 2010). This paper presents results of a pilot numerical

study of CFS deck in bending performed using nonlinear FE deck models developed in ANSYS and validated using available test data.

Trapezoidal deck profiles with different heights and thicknesses commonly used in the US were studied. Compression flanges of the profiles were either flat or had longitudinal intermediate stiffeners of different sizes. The effects of boundary conditions on the critical elastic buckling moment and the ultimate flexural strength of the decks were studied, as well as the effects of yield stress and steel material models on the deck ultimate flexural strength. The deck elastic buckling and ultimate moments obtained in this study were compared with those calculated in accordance with the DSM and EWM equations given in AISI S100-16. The results of the parametric study were used as a basis for the formulation of new design equations for predicting local elastic buckling coefficients of the deck compression flanges and for improving modifications of DSM for deck with flat compression flanges failing in local and distortional buckling. The main objectives of this study were to get a better understanding of the deck flexural behavior and to explore possibilities for improvement of the existing DSM equations for steel deck.

## 2. Development and validation of finite element models

FE deck models were developed, calibrated, and validated using steel deck profiles shown in Fig. 1. These profiles were physically tested at the Karlsruhe Institute of Technology (KIT) for the GRISPE research project (Fauth 2015). In the project, 14 non-perforated single-sheet, single-span deck panels spanning 3300 mm were tested in six-point bending, which simulated a uniformly distributed load, in accordance with EN 1993-1-3:2006. The deck had a nominal thickness of 0.75 and 1.00 mm and a nominal yield stress of 320 MPa. To prevent deck web crippling failures, the load was applied to the deck bottom flanges via timber blocks, while support reactions were applied to the deck top flanges also through timber blocks. Transverse ties were installed at the load locations and near deck supports to prevent deck sheets from spreading under applied load.

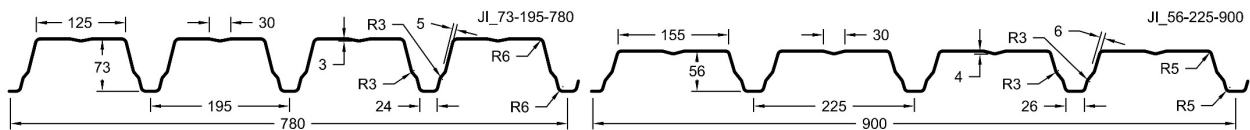


Figure 1: Dimensions [mm] of deck profiles used for model validation

FE models of the tested deck profiles were created in a commercial general-purpose software ANSYS using actual base steel thickness and actual mechanical properties of the steel reported by Fauth (2015). Corner radii at the intersections of the deck top and bottom flanges with the deck webs were included in the models, whereas the web and top flange stiffeners were modeled with sharp corners. The deck was modeled with four-node structural shell elements, SHELL181, with five integration points and six degrees of freedom at each node.

The deck material behavior was defined by multilinear isotropic hardening models (MISO) with von Mises plasticity. The deck stress-strain diagrams were described by the nonlinear models proposed by Gardner and Yun (2018) with key input parameters determined from actual yield and tensile strengths of the steel reported by Fauth (2015). An elastic modulus of  $2.03 \times 10^5$  MPa and a Poisson's ratio of 0.3 were specified. The true stresses and strains, calculated from the engineering stresses and strains according to Appendix C.6 of EN 1993-1-5:2006, were used in the models.

Deck models were meshed with quadrilateral elements with the maximum sizes of 5 and 10 mm in the directions across and along the deck span, respectively. This mesh density was determined from a convergence study to be optimal from the accuracy and computational efficiency standpoints (Degtyarev 2020).

Figure 2 shows boundary conditions of the FE deck models. Only one-half of the deck sheet was modeled due to the symmetry in the boundary and loading conditions. The ANSYS symmetry degree-of-freedom constraints were applied to the nodes at the deck mid-span. Vertical translations of the deck top flange nodes were restrained at the deck support. Lateral displacement of one node at the deck bottom flange edge was restrained to prevent rigid body motion. The deck models were loaded by forces applied to deck bottom flanges. Vertical displacements of deck bottom flange nodes at the load locations were coupled. Transverse ties were modeled by coupling lateral displacements of nodes at the deck panel edges at the load locations and near deck supports.

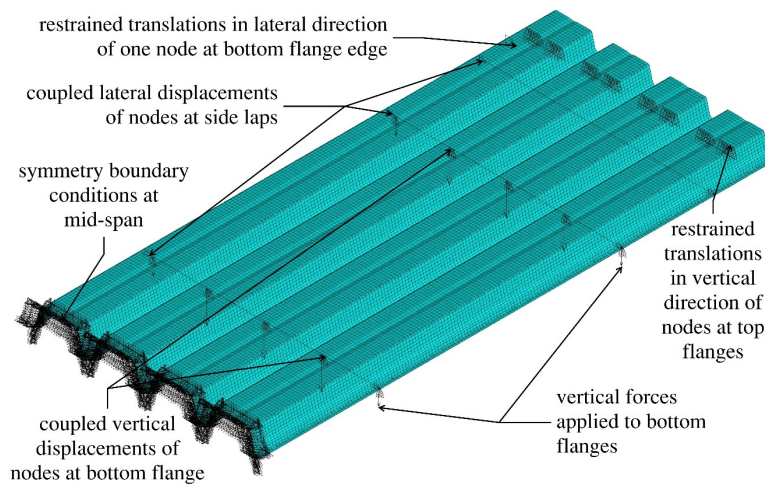


Figure 2: Boundary conditions of deck used for model validation

Deck models were analyzed in two steps. Elastic buckling analyses conducted to obtain elastic buckling modes and moments were followed by nonlinear static analyses performed to obtain ultimate moment capacities. The nonlinear static analyses were carried out on the models that included initial geometric imperfection (IGI) distributions based on the first elastic buckling mode obtained from the elastic buckling analysis. The first elastic buckling mode of the models was distortional buckling of the deck compression flanges characterized by vertical deformations of the top flange longitudinal stiffener. The IGI magnitude of  $b_{tf}/150$ , where  $b_{tf}$  is deck top flange width, was specified in the model based on a study of different IGI magnitudes presented elsewhere (Degtyarev 2020). The absolute IGI magnitudes were 0.83 and 1.03 mm for the 73 and 56 mm deep decks, respectively. Large-deflection effects were included into the FE models to account for the geometric nonlinearity.

Comparisons of deck load-deflection diagrams and ultimate moments obtained from the tests and the FE simulations presented in Figs. 3 and 4, respectively, show very good agreements between the experimental and numerical data. The 1<sup>st</sup> and 3<sup>rd</sup> deliveries shown in Fig. 3 refer to deck made from different coils of steel and delivered to the testing laboratory at different times (Fauth 2015). In Fig. 4,  $M_{u,test}$  and  $M_{u,FEA}$  are ultimate moments from tests and FE simulations, respectively.

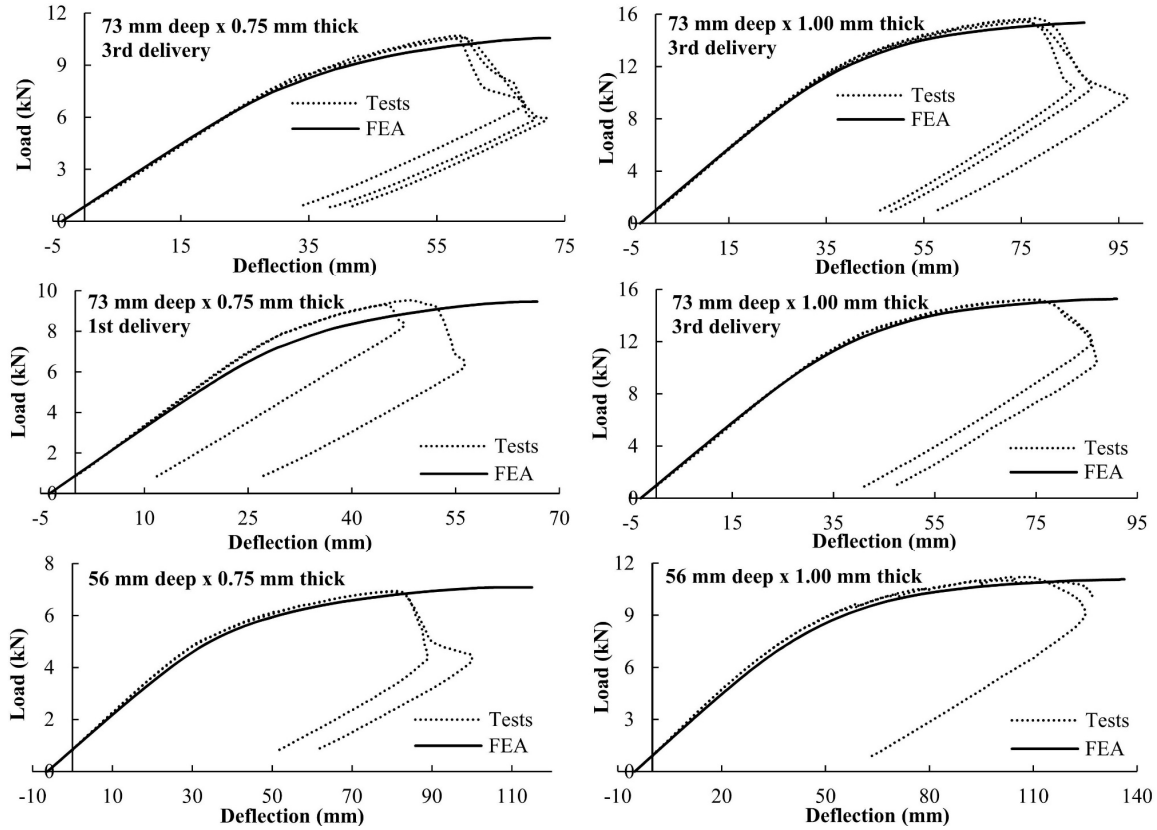


Figure 3: Load-deflection diagrams from tests and FE simulations

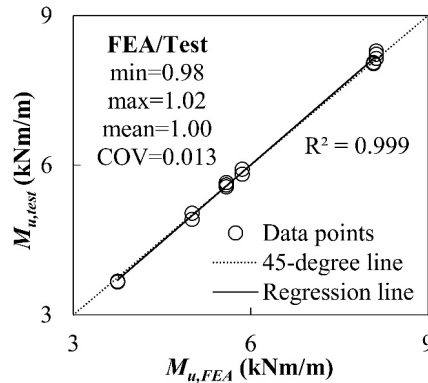


Figure 4: Comparison of ultimate moments from tests and FE simulations

Based on these results, it can be concluded that the developed FE models can predict the structural response and the ultimate moment capacity of steel deck well. Therefore, the developed FE deck models can be used for parametric studies of CFS deck in bending.

### 3. Numerical parametric studies

The developed FE deck models were used for numerical parametric studies of elastic buckling and post-buckling strength of CFS deck profiles manufactured in the US. Figure 5 shows deck profiles considered in the parametric studies. They included 25 mm deep 1F form deck, 38 and 77 mm deep 1.5B and 3N roof decks, and 53 and 77 mm deep 2C and 3C composite decks with 2 different sizes of flange stiffeners. Several modified profiles were also considered. To study the effects of

top flange stiffeners on the elastic buckling and post-buckling strength, top flange stiffeners of two different sizes were added to 1.5B deck. The modified profiles are referred to as 1.5BST1 and 1.5BST2. To study the effects of the level of deck non-symmetry on the elastic buckling and post-buckling strength, the bottom flanges of 1.5B and 3N decks were made wider, so their widths were equal to the widths of the top flanges. These modified profiles were denoted as 1.5BR and 3NR. Four steel thicknesses were considered for each studied deck: 0.45, 0.60, 0.75, and 0.91 mm (26, 24, 22, and 20 GA, respectively) for 1F deck and 0.75, 0.91, 1.20, and 1.52 mm (22, 20, 18, and 16 GA, respectively) for all other decks. All decks were simply-supported with span lengths of 1219, 1829, 2438, and 3658 mm for profiles with depths of 25, 38, 53, and 77 mm, respectively.

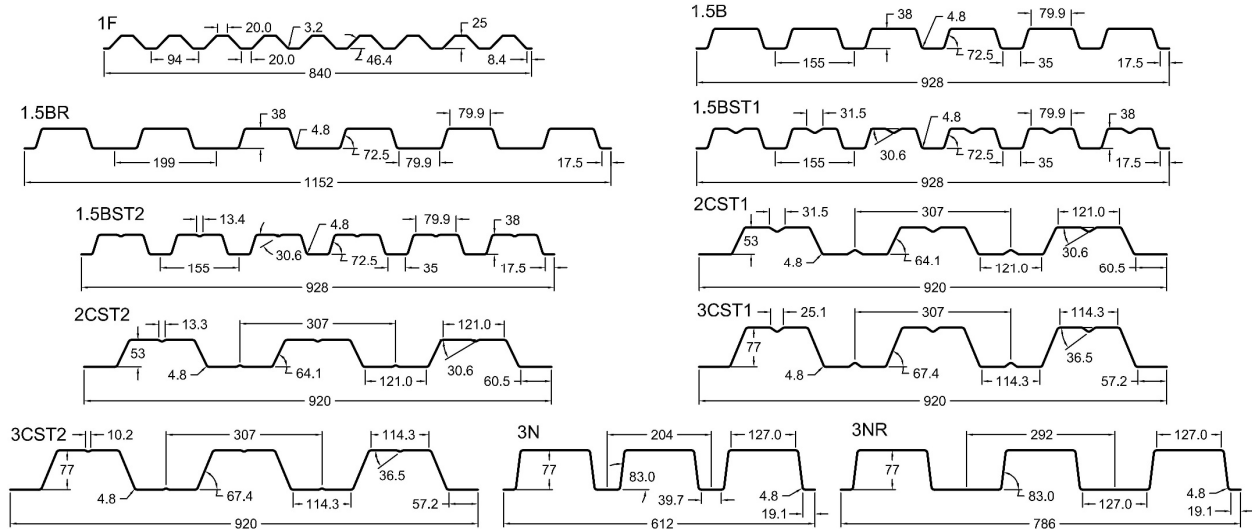


Figure 5: Dimensions [mm] of deck profiles used in parametric studies

The parametric study was carried out in two phases. In Phase 1, the effects of deck boundary conditions and transverse ties on the elastic buckling and post-buckling strength of the deck were studied. In Phase 2, the effects of steel constitutive models, yield stress, and deck profile geometry on the elastic buckling and post-buckling strength were evaluated using the FE deck models with boundary conditions selected based on the results from Phase 1. Overall, 32 and 440 FE deck models were created and analyzed in Phases 1 and 2, respectively.

### 3.1 Effects of boundary conditions and transverse ties

The effects of deck boundary conditions and transverse ties were studied on two deck profiles, 1F and 3CST1, which represent the shallowest and deepest decks considered in the study. 1F deck has flat flanges, while 3CST1 deck has one longitudinal intermediate stiffener in each flange. A yield stress of 276 MPa and the elastic-perfectly plastic material behavior of steel were specified.

Two different boundary conditions shown in Fig. 6 were evaluated. In the top-flange-supported-bottom-flange-loaded (TFS-BFL) models (Fig. 6a), the loads were applied to the deck bottom flanges and the support reactions were transferred to the deck top flanges as in the physical tests described above. In the bottom-flange-supported-top-flange-loaded (BFS-TFL) models (Fig. 6b), the loads were applied to the deck top flanges and the support reactions were transferred to the deck bottom flanges. In the BFS-TFL models, deck webs are in compression, which may result in web crippling contributing to the elastic buckling and post-buckling strength of the deck. In the TFS-BFL models, deck web crippling is not a factor, because the deck webs are in tension.

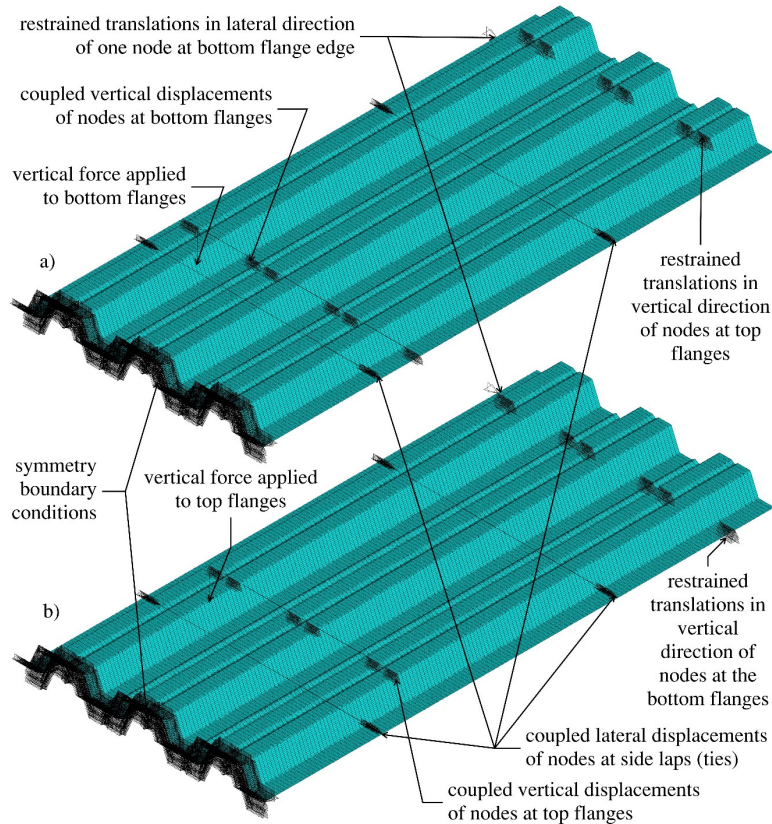


Figure 6: Deck boundary conditions for a) TFS-BFL and b) BFS-TFL models

Figure 6 shows FE models with transverse ties, which were provided at 914 mm on center in accordance with the maximum deck side lap connection spacing allowable in the US. The first ties were specified at 152 and 457 mm from the support for 1F and 3CST1 decks, respectively, to ensure that the tie locations were symmetrical about the deck mid-span and that no tie was provided at the deck mid-span. The models without transverse ties (not shown in Fig. 6) were also analyzed.

All other characteristics of the TFS-BFL and BFS-TFL models were similar. Only one-half of the deck span deck was modeled with the symmetry boundary conditions at the mid-span. The FE models simulated four-point bending tests with loads applied as forces at  $L/3$  from the deck supports, where  $L$  is deck span. Vertical displacements of the deck flange nodes at the load locations were coupled. All other parameters of the FE models were the same as described in Section 2.

The first elastic buckling mode for 1F decks with flat compression flanges was local buckling of the compression flanges shown in Fig. 7a. 3CST1 decks demonstrated both the distortional and local buckling of the compression flanges with longitudinal intermediate stiffeners shown in Figs. 7b and 7c. For the 0.75 and 0.91 mm thick decks, the local buckling preceded the distortional buckling, whereas the distortional buckling mode came first for the 1.20 and 1.52 mm thick decks.

Figure 8 shows the effects of the boundary conditions and transverse ties on the elastic buckling and ultimate moments. In Fig. 8,  $M_{crl}$ ,  $M_{crd}$ , and  $M_u$  are local buckling, distortional buckling, and ultimate moments, respectively, from FE simulations. The differences in the boundary conditions and transverse ties did not affect the elastic buckling moments of shallow 1F decks with all

considered thicknesses. For this deck, the ultimate moments for the BFS-TFL models were smaller than those for the TFS-BFL models by 2-7% and 3-9% for the models with and without transverse ties, respectively. The ultimate moment capacity reduction increased when the deck thickness reduced. The reduction in the ultimate moments is attributed to the effects of the deck web crippling on the ultimate moment capacity, which was more pronounced in the lighter deck models without transverse ties. For the TFS-BFL models of 1F deck, transverse ties did not affect the ultimate moment. For the BFS-TFL models of 1F deck, transverse ties resulted in a small, 1-4 %, increase in the ultimate moments.

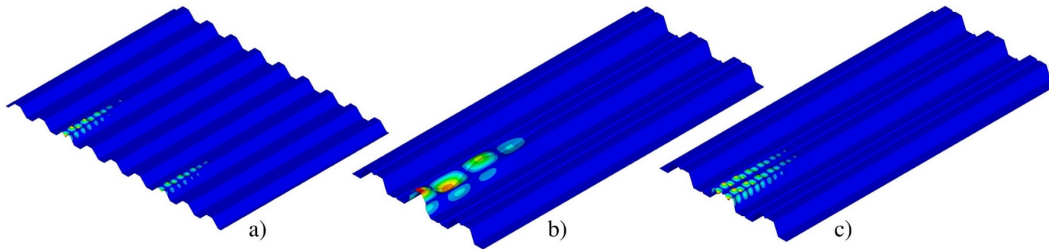


Figure 7: Elastic buckling modes: a) local buckling of flat compression flanges, b) distortional and c) local buckling of compression flanges with longitudinal intermediate stiffeners

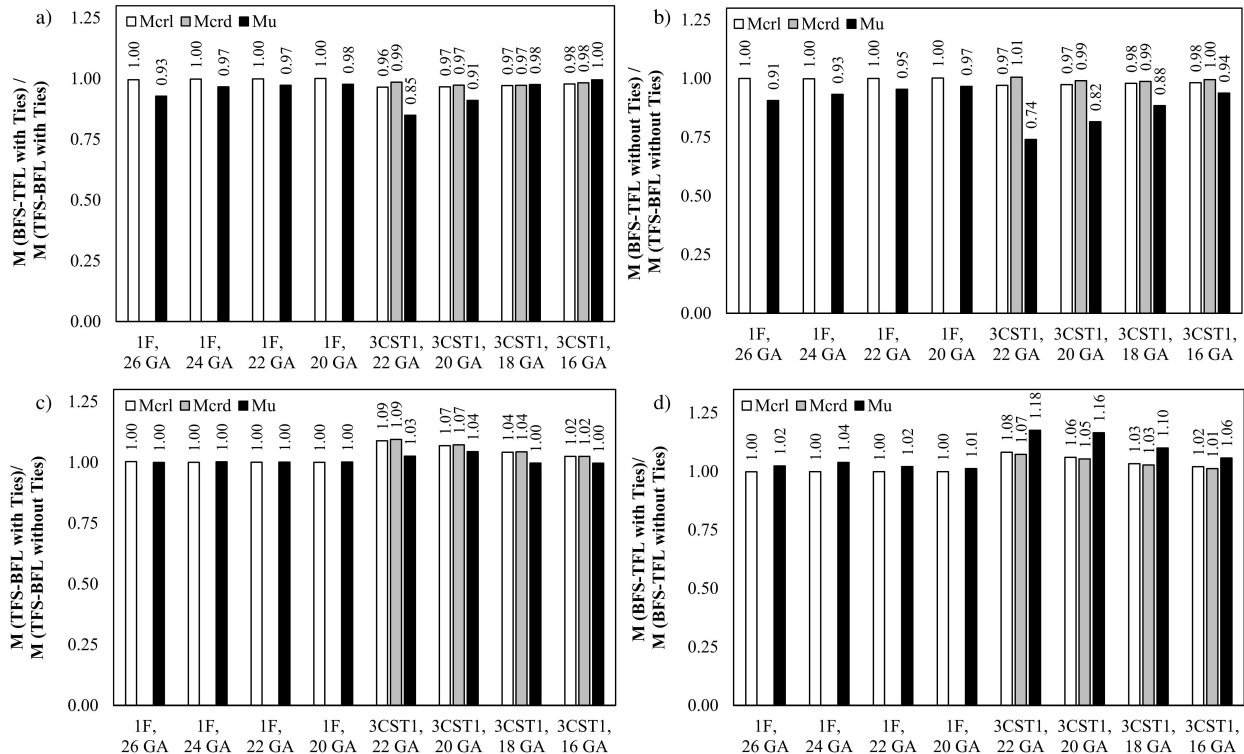


Figure 8: Effects of boundary conditions and transverse ties on elastic buckling and ultimate moments

The BFS-TFL models of 3CST1 deck with and without ties showed 2-4% greater local elastic buckling moments than the TFS-BFL models. The distortional elastic buckling moments of the BFS-TFL models were 1-3% smaller than those for the TFS-BFL models when transverse ties were provided. For 3CST1 deck with both considered boundary conditions, the distortional elastic buckling moments were approximately equal when no ties were provided. The ultimate moments of the BFS-TFL models of 3CST1 deck with and without ties were up to 15 and 26%, respectively, smaller than the ultimate moments for the TFS-BFL models. Greater ultimate moment reductions

were observed for lighter deck. The addition of ties to the models of 3CST1 deck with both considered boundary conditions resulted in increases in the elastic buckling and ultimate moments. The increases in the elastic buckling moments were approximately the same for the TFS-BFL and BFS-TFL models, whereas the BFS-TFL models showed significantly greater increases in the ultimate moment capacities than the TFS-BFL models (6-18% vs. 0-4%). Greater increases in the elastic buckling and ultimate moments of 3CST1 deck were obtained for lighter deck profiles.

The presented results show that the boundary conditions and the transverse ties may affect the elastic buckling and ultimate moments of deck, especially the one with slender webs. Therefore, appropriate boundary conditions should be used in laboratory testing and numerical simulations to obtain accurate results. The TFS-BFL models without ties were selected for further parametric studies. These models exclude the effects of web crippling on the deck flexural strength and provide true moment capacities of the deck. Due to the relatively small effects of the ties on the elastic buckling and ultimate moments in the TFS-BFL models (see Fig. 8c), the transverse ties were not included in the parametric study models.

### 3.2 Effects of steel constitutive models, yield stress, and deck profile geometry

In this phase, FE models were created and analyzed for all deck profiles shown in Fig. 5. Four different steel yield strengths—228, 276, 345, and 414 MPa—were studied. Three different steel material models—elastic-perfectly plastic, bilinear, and nonlinear—were examined. The nonlinear material models were described by formulas proposed by Gardner and Yun (2018). 1F, 1.5BR, 2CST1, 2CST2, 3CST1, 3CST2, and 3NR symmetrical profiles, as well as 1.5BST2 deck were analyzed only in the normal orientation bending with the deck top flanges in compression. 1.5B, 1.5BST1, and 3N non-symmetrical profiles were analyzed in the normal and inverted orientation bending with the wider upper flanges in compression and tension, respectively.

#### 3.2.1 Deck profiles with flat compression flanges

In this section, results for 1F, 1.5B, 1.5BR, 3N, and 3NR decks in the normal orientation and 1.5B, 1.5BST1, and 3N deck in the inverted orientation bending are presented and discussed.

##### 3.2.1.1 Elastic buckling

Flat compression flanges of all decks in the normal orientation bending were longitudinally stiffened by deck webs. These profiles demonstrated local elastic buckling modes of compression flanges similar to the one shown in Fig. 7a. The edge compression flanges of the deck in the inverted orientation bending were unstiffened along one edge and demonstrated both local and distortional elastic buckling modes (Fig. 9).

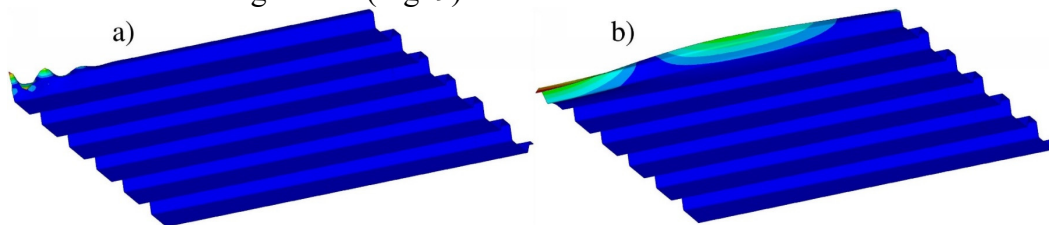


Figure 9. Elastic buckling modes of unstiffened flat compression flanges of profiles loaded in the inverted orientation bending: a) local and b) distortional buckling

Buckling coefficients of flat deck flanges in compression were determined from local elastic buckling moments obtained from the FE simulations using the following equation:

$$k = \frac{M_{crl,FEA}}{S_f} \frac{12(1-\mu^2)}{\pi^2 E} \left(\frac{w}{t}\right)^2 \quad (1)$$

where  $M_{crl,FEA}$  is local elastic buckling moment from FE simulations,  $S_f$  is section modulus of full deck section for compression deck flange,  $\mu$  is Poisson's ratio of steel,  $E$  is modulus of elasticity of steel,  $w$  is flat width of deck flange, and  $t$  is deck thickness.

Figure 10 shows buckling coefficients for flat stiffened and unstiffened compression flanges of deck calculated with Eq. (1) as functions of the relative compression zone depth,  $Y_{na}/h_d$ , where  $Y_{na}$  is vertical distance from deck compression flange to neutral axis of full deck section and  $h_d$  is deck height. Buckling coefficients for flat stiffened and unstiffened plates specified in AISI S100-16 (4 and 0.43, respectively) are also shown in Fig. 10.

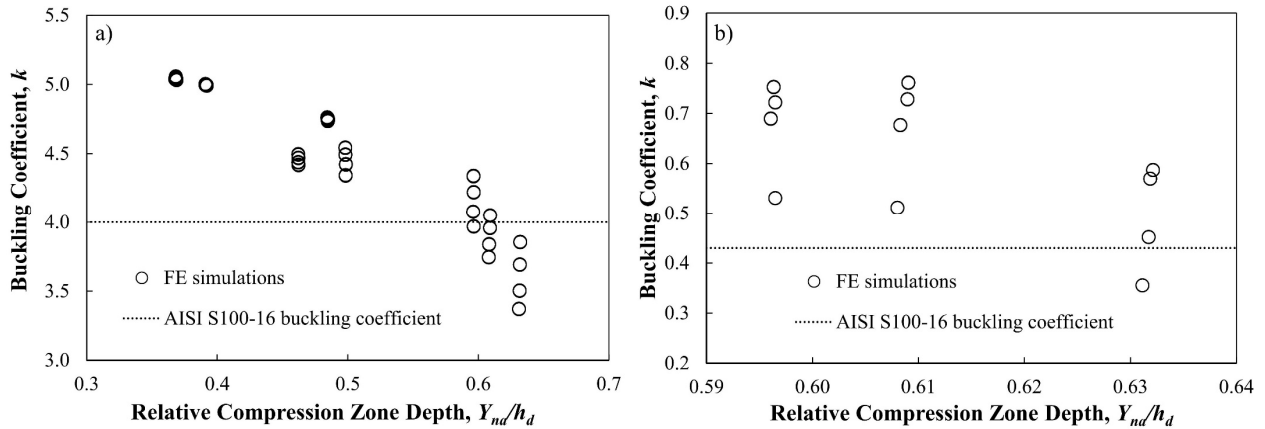


Figure 10. Buckling coefficients for deck flat compression flanges: a) stiffened and b) unstiffened flanges

Figure 10 shows that buckling coefficients for stiffened flanges increased when  $Y_{na}/h_d$  decreased. When  $Y_{na}/h_d$  was smaller than 0.6, the deck buckling coefficients were greater than the buckling coefficient for a long simply supported plate. When  $Y_{na}/h_d$  was greater than 0.6, the deck buckling coefficients were smaller than the buckling coefficient for a long simply supported plate. A similar trend was observed for the unstiffened flanges. The buckling coefficient reduced when  $Y_{na}/h_d$  increased. This can be explained by the interaction between flanges and webs of the deck and by the contribution of deck webs to the flange rigidity. As Fig. 10 shows, the web contribution reduced when  $Y_{na}/h_d$  increased. When the web compression zone became large, which corresponded to  $Y_{na}/h_d$  of 0.60 and 0.63 for stiffened and unstiffened flanges, respectively, buckling of the compression part of the web appears to have a negative effect on the compression flange buckling, which made the buckling coefficients smaller than the values for simply supported plates.

The  $M_{crd,FEA}/M_{crl,FEA}$  ratios, where  $M_{crd,FEA}$  is distortional elastic buckling moment from FE simulations, ranged from 0.77 to 1.74 and from 0.66 to 1.31 for the 38 and 77 mm deep deck profiles, respectively. The  $M_{crd,FEA}/M_{crl,FEA}$  ratios reduced when the deck thickness increased.

### 3.2.1.2 Post-buckling strength

The deck ultimate moments obtained from the FE simulations were compared with the deck flexural strengths calculated using DSM and EWM of AISI S100-16. Table 2 compares the  $M_{u,FEA}/M_{u,DSM}$  ratios for the FE models with different stress-strain relationships of steel, where  $M_{u,FEA}$  and  $M_{u,DSM}$  are ultimate deck moments predicted by FE simulations and DSM. Table 2 shows that models with the nonlinear steel stress-strain curves predicted slightly greater (up to 4%

on average) ultimate moments when compared with the elastic-perfectly plastic and bilinear models. The nonlinear stress-strain diagrams also demonstrated slightly smaller scatter of the  $M_{u,FEA}/M_{u,DSM}$  ratios characterized by smaller COVs. Overall, the differences in the ultimate moments predicted by FE models with the studied steel material models were relatively small. Therefore, the FE simulation results for the nonlinear steel models only were used in further analyses. Table 2 also shows that the  $M_{u,FEA}/M_{u,DSM}$  ratios were relatively high indicating that DSM adopted in AISI S100-16 may be overly conservative for decks with flat compression flanges.

Table 2: Summary of  $M_{u,FEA}/M_{u,DSM}$  values for deck with flat flanges in compression

SSR <sup>1</sup>	Elastic-Perfectly Plastic				Bilinear				Nonlinear			
$F_y$ (MPa)	228	276	345	414	228	276	345	414	228	276	345	414
min	1.01	1.04	1.04	1.04	1.01	1.04	1.04	1.04	1.09	1.09	1.09	1.09
max	1.43	1.49	1.55	1.60	1.44	1.49	1.55	1.60	1.37	1.43	1.51	1.55
mean	1.18	1.18	1.20	1.22	1.19	1.19	1.20	1.22	1.22	1.22	1.22	1.22
COV <sup>2</sup>	0.096	0.105	0.116	0.122	0.098	0.105	0.117	0.122	0.077	0.083	0.098	0.113

Notes: 1. SSR stands for stress-strain relationship of steel; 2. COV stands for coefficient of variation.

Figure 11 compares the FE strength predictions for the deck profiles with flat compression flanges with the AISI S100-16 local and distortional buckling strength curves, and the elastic buckling curve described by Eqs. (2), (3), and (4), respectively.

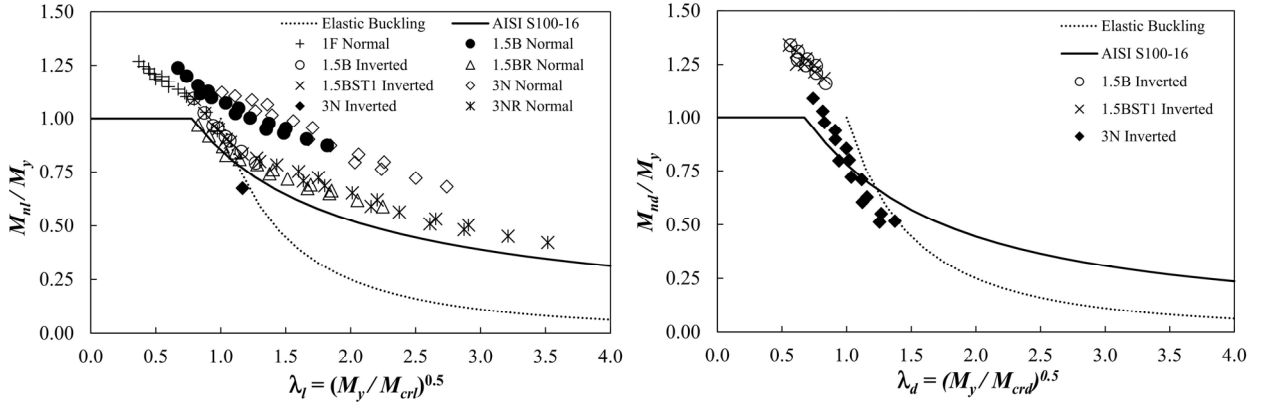


Figure 11: Strength curves and FE predictions for a) local and b) distortional buckling of deck with flat flanges in compression

$$\frac{M_{nl}}{M_y} = \begin{cases} 1 & \text{for } \lambda_l \leq 0.776 \\ \left[ 1 - 0.15 \left( \frac{1}{\lambda_l^2} \right)^{0.4} \right] \left( \frac{1}{\lambda_l^2} \right)^{0.4} & \text{for } \lambda_l > 0.776 \end{cases} \quad (2)$$

$$\frac{M_{nd}}{M_y} = \begin{cases} 1 & \text{for } \lambda_d \leq 0.673 \\ \left[ 1 - 0.22 \left( \frac{1}{\lambda_d^2} \right)^{0.5} \right] \left( \frac{1}{\lambda_d^2} \right)^{0.5} & \text{for } \lambda_d > 0.673 \end{cases} \quad (3)$$

$$\frac{M_{nl}}{M_y} = \frac{1}{\lambda_l^2}, \quad \frac{M_{nd}}{M_y} = \frac{1}{\lambda_d^2} \quad (4)$$

where  $M_{nl}$  and  $M_{nd}$  are nominal flexural strengths (ultimate moments from FE simulations) for local and distortional buckling, respectively;  $M_y$  is yield moment of full section;  $\lambda_l = \sqrt{M_y/M_{crit}}$

and  $\lambda_d = \sqrt{M_y/M_{crd}}$  are slenderness factors of local and distortional buckling, respectively;  $M_{cr}$  is critical elastic local buckling moment; and  $M_{crd}$  is distortional elastic buckling moment.

Figure 11 shows that the ultimate moments for local buckling from the FE simulations were considerably greater than the elastic buckling moment capacities for  $\lambda_l > 1.25$ , which indicates that the deck profiles, especially the ones with large local buckling slenderness, exhibited significant post-buckling strength. The DSM local buckling strength predictions were conservative for the majority of the studied decks and overly conservative for the non-symmetrical decks (1.5B and 3N) with wider flanges in compression. These results are very similar to the Winter test results discussed by Schafer and Peköz (1998). It is interesting to note that the symmetrical decks with slender compression flanges of the same widths as the tension flanges (1.5BR and 3NR) showed smaller differences between the flexural strengths predicted by DSM and the FE simulations when compared with the non-symmetrical profiles (1.5B and 3N). These results indicate that the local post-buckling strength of decks with flat compression flanges depends not only on the compression flange slenderness, but also on the level of deck non-symmetry.

The FE-predicted ultimate moments for distortional buckling of decks with  $\lambda_d \leq 1$  were slightly greater than those predicted by DSM. For decks with  $\lambda_d > 1$ , DSM predicted slightly greater strengths than those obtained from the FE simulations. The FE ultimate moments were below the elastic distortional buckling curve, which indicates that the studied profiles with flat unstiffened compression flanges did not exhibit the distortional post-buckling strength. Figure 11 also shows that decks with flat flanges and small slenderness ratios demonstrated significant inelastic reserve strength of up to 35%, further analysis of which was beyond the scope of this study.

Figure 12 shows dependence of the  $M_{u,FEA}/M_{u,DSM}$  ratios from deck local and distortional slenderness and comparison statistics between the FE and DSM predictions. The  $M_{u,FEA}/M_{u,DSM}$  ratios range from 0.88 to 1.66 with the mean value of 1.24 for local buckling and from 0.78 to 1.34 with the mean value of 1.15 for distortional buckling. These results indicate that there is a room for improvement of the current DSM provisions for steel deck with flat compression flanges.

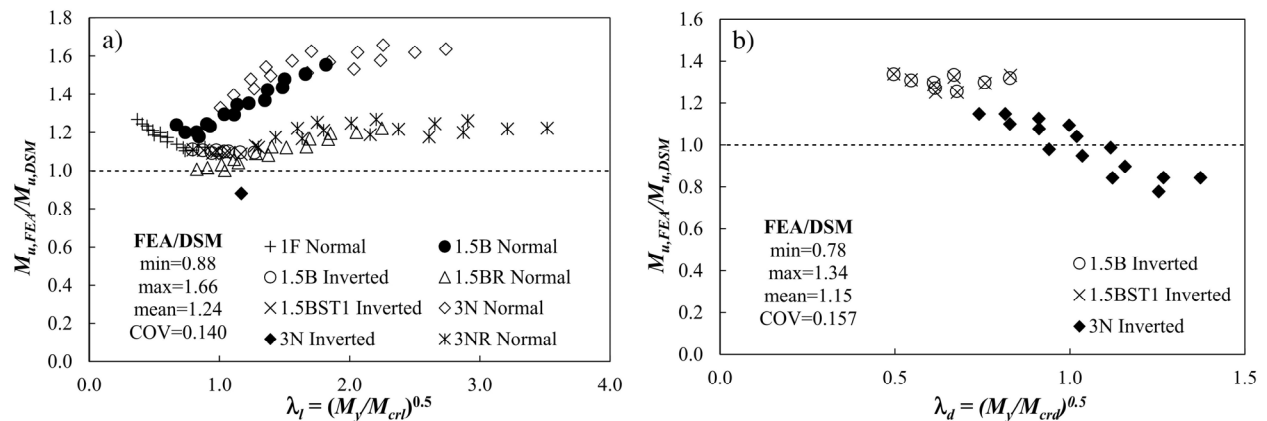


Figure 12: Effects of slenderness on  $M_{u,FEA}/M_{u,DSM}$  for a) local and b) distortional buckling of deck with flat compression flanges

Figure 13 shows dependence of the  $M_{u,FEA}/M_{u,EWM}$  ratios from deck local and distortional slenderness and comparison statistics between the FE and EWM predictions. On average, EWM

shows a better agreement with the FE predictions for deck with flat compression flanges than DSM. The  $M_{u,FEA}/M_{u,EWM}$  ratios range from 0.75 to 1.27 with the mean value of 1.05 for local buckling and from 0.65 to 1.34 with the mean value of 1.05 for distortional buckling. However, moment capacities of deck failing in distortional buckling predicted by EWM were not conservative for deck with  $\lambda_d > 1.0$ . The scatter of  $M_{u,FEA}/M_{u,EWM}$  was considerably greater than the scatter of  $M_{u,FEA}/M_{u,DSM}$  for distortional buckling. It is also interesting to note that for local buckling the  $M_{u,FEA}/M_{u,EWM}$  values decrease when the slenderness factor increases, whereas the  $M_{u,FEA}/M_{u,DSM}$  values decrease when  $\lambda_l < 0.8$ , increase when  $0.8 < \lambda_l \leq 2.0$ , and stay approximately the same when  $\lambda_l > 2.0$ .

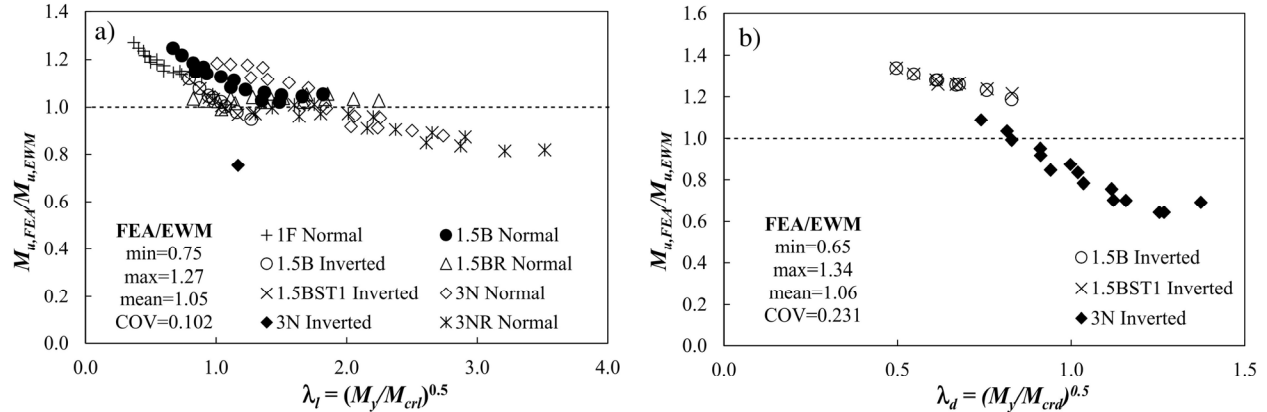


Figure 13: Effects of slenderness on  $M_{u,FEA}/M_{u,EWM}$  for a) local and b) distortional buckling of deck with flat compression flanges

The  $Y_{na}/h_d$  ratio can be considered as a measure of the deck non-symmetry level, alternative to the deck flange widths ratio. The former is deemed to be more convenient for decks with longitudinal intermediate flange stiffeners, because  $Y_{na}/h_d$  depends on the stiffener size and shape, whereas the flange width ratio does not. The  $M_{u,FEA}/M_{u,DSM}$  and  $M_{u,FEA}/M_{u,EWM}$  ratios for local buckling plotted against  $Y_{na}/h_d$  in Fig. 14 show dependence of  $M_{u,FEA}/M_{u,DSM}$  from  $Y_{na}/h_d$  when the latter is in the range from 0.37 to 0.50 and independence of  $M_{u,FEA}/M_{u,EWM}$  from  $Y_{na}/h_d$ .

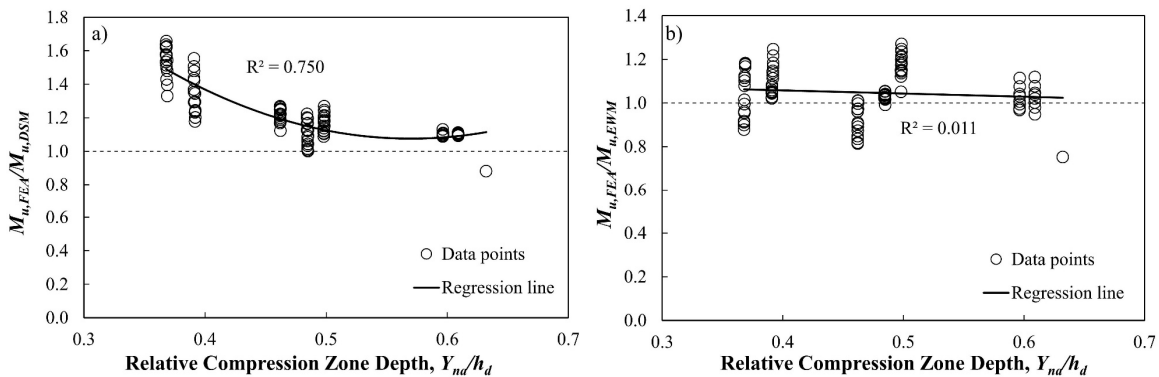


Figure 14: Effects of relative compression zone depth of deck with flat flanges on a)  $M_{u,FEA}/M_{u,DSM}$  and b)  $M_{u,FEA}/M_{u,EWM}$  governed by local buckling

### 3.2.2 Deck profiles with longitudinal intermediate stiffeners in compression flanges

In this section, results for 1.5BST1, 1.5BST2, 2CST1, 2CST2, 3CST1, and 3CST2 decks in the normal orientation bending are presented and discussed.

### 3.2.2.1 Elastic buckling

The decks with longitudinal intermediate stiffeners in compression flanges demonstrated distortional and local elastic buckling modes similar to the ones shown in Figs. 7b and 7c. For the decks with larger stiffeners (1.5BST1, 2CST1, and 3CST1), local elastic buckling preceded distortional buckling for steel thicknesses of 0.75 and 0.91 mm, whereas distortional buckling occurred first for the 1.20 and 1.52 mm thick decks. In the decks with smaller stiffeners (1.5BST2, 2CST2, and 3CST2), distortional buckling was observed first for all considered thicknesses.

Figure 15 compares local and distortional buckling moments of the studied decks obtained from the FE simulations and calculated in accordance with AISI S100-16 as follows:

$$M_{crl} = S_f k_{loc} \frac{\pi^2 E}{12(1-\mu^2)} \left(\frac{t}{w}\right)^2 \quad (5)$$

$$M_{crd} = S_f k_d \frac{\pi^2 E}{12(1-\mu^2)} \left(\frac{t}{w}\right)^2 \quad (6)$$

where  $k_{loc}$  and  $k_d$  are plate buckling coefficients for local and distortional buckling calculated as described in Appendix 1 of AISI S100-16.

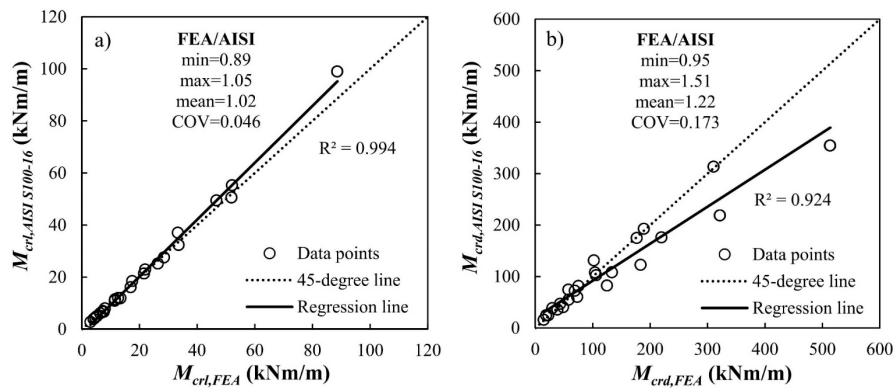


Figure 15: Comparisons of a) local and b) distortional buckling moments of deck with longitudinal intermediate stiffeners in compression flanges from FE simulations and AISI S100-16 predictions

Figure 15 shows that the deck local buckling moments predicted by Eq. (5) agreed very well with the FE predictions. The deck distortional buckling moments predicted by Eq. (6), on the other hand, were considerably smaller than the distortional buckling moments from the FE simulations.

### 3.2.2.2 Post-buckling strength

Table 3 compares the  $M_{u,FEA}/M_{u,DSM}$  ratios for the FE models with different steel material diagrams. The nonlinear relationship resulted in slightly smaller values of the deck flexural strength and a greater scatter of the  $M_{u,FEA}/M_{u,DSM}$  ratios than the elastic-perfectly plastic and bilinear models. DSM predicted the flexural strength of the deck with longitudinal intermediate stiffeners better than the strength of the deck with flat flanges. The FE simulation results for the nonlinear steel models only were used in further analyses due to the relatively small differences in the deck strengths predicted by the models with the considered different steel constitutive models.

Figure 16 compares the FE strength predictions with the AISI S100-16 local and distortional strength curves, and the elastic buckling curve. The FE-predicted ultimate moments for local buckling were below the DSM strength curve, which indicates a slight non-conservatism of DSM

in predicting flexural strength of decks with longitudinal intermediate flange stiffeners failing in local buckling. Figure 16b shows that DSM agreed with the parametric study results for the deck failing in distortional buckling reasonably well. It gave, however, overly conservative predictions for 1.5BST2 deck, which is a non-symmetrical deck with small stiffeners. Due to the relatively small size of the stiffeners, the buckling and failure modes of 1.5BST2 deck were similar to those of 1.5B deck. Figure 16 also shows that the deck sections with  $\lambda_l < 1.2$  failing in local and distortional buckling exhibited the inelastic buckling failure mode. Deck sections with small slenderness ratios showed inelastic buckling reserve strength of up to 35%.

Table 3: Summary of  $M_{u,FEA}/M_{u,DSM}$  values for deck with longitudinal intermediate stiffeners in compression flanges

SSR <sup>1</sup>	Elastic-Perfectly Plastic				Bilinear				Nonlinear			
	$F_y$ (MPa)	228	276	345	414	228	276	345	414	228	276	345
min	0.95	0.97	0.97	0.93	0.96	0.97	0.98	0.93	0.86	0.88	0.89	0.86
max	1.28	1.27	1.26	1.24	1.30	1.29	1.27	1.26	1.36	1.33	1.30	1.27
mean	1.08	1.08	1.08	1.07	1.09	1.09	1.08	1.07	1.05	1.04	1.03	1.01
COV <sup>2</sup>	0.118	0.108	0.096	0.093	0.120	0.111	0.099	0.100	0.171	0.157	0.142	0.134

Notes: 1. SSR stands for stress-strain relationship of steel; 2. COV stands for coefficient of variation.

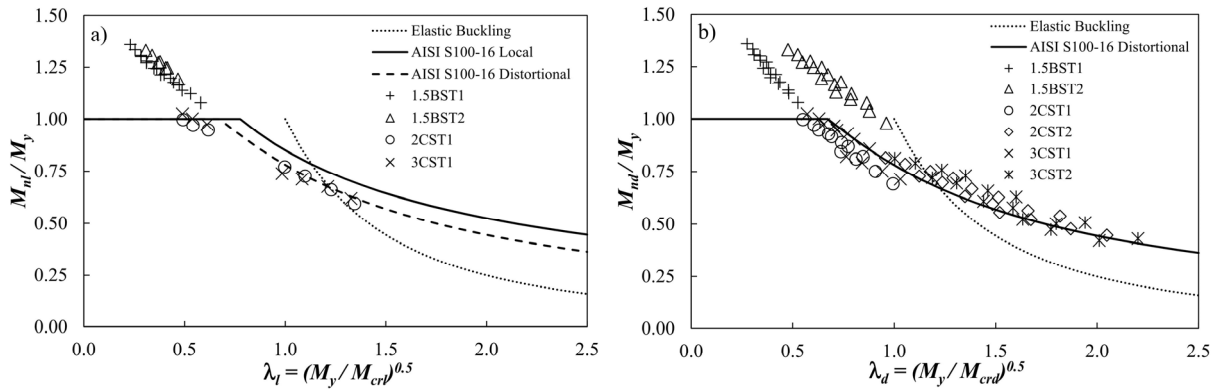


Figure 16: Strength curves and FE predictions for a) local and b) distortional buckling of deck with longitudinal intermediate stiffeners in compression flanges

The  $M_{u,FEA}/M_{u,DSM}$  and  $M_{u,FEA}/M_{u,EWM}$  ratios plotted as functions of deck slenderness in Figs. 17 and 18 show that DSM and EWM resulted in almost identical predictions of the deck local buckling strength. EWM, however, resulted in less conservative results for the deck distortional buckling strength, especially for the slender deck sections.

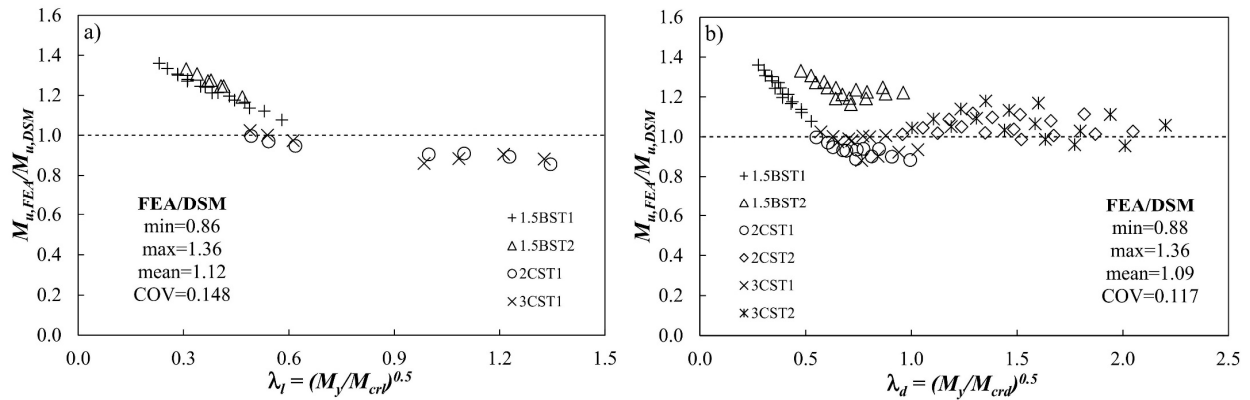


Figure 17: Effects of slenderness on  $M_{u,FEA}/M_{u,DSM}$  for a) local and b) distortional buckling of deck with longitudinal intermediate stiffeners in compression flanges

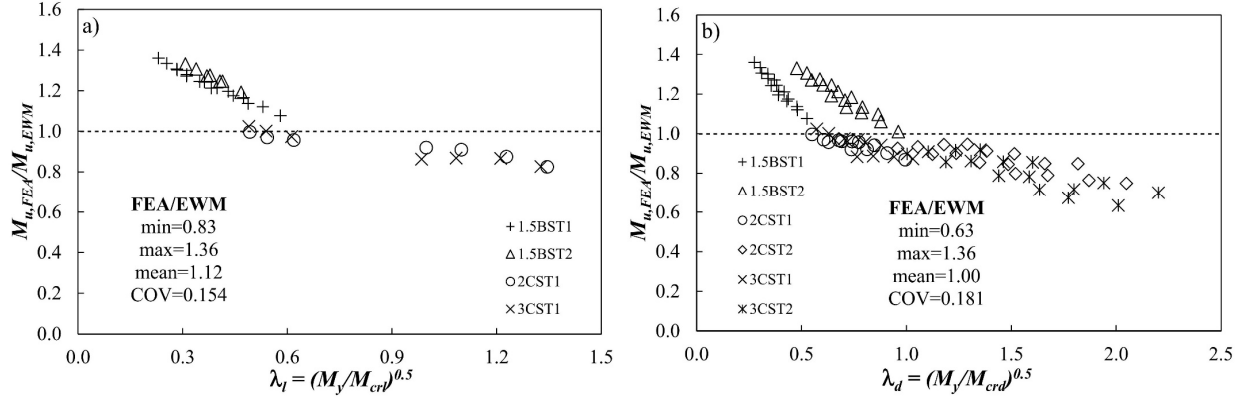


Figure 18: Effects of slenderness on  $M_{u,FEA}/M_{u,EWM}$  for a) local and b) distortional buckling of deck with longitudinal intermediate stiffeners in compression flanges

#### 4. Design recommendations

Regression analyses of the obtained results allowed for the development of design equations for predicting local and distortional buckling coefficients for deck profiles with flat and longitudinally stiffened compression flanges, respectively. Revised DSM equations for local and distortional buckling of deck with flat compression flanges were also developed. The developed equations are applicable to the profiles considered in this study.

Local buckling coefficients of the deck with flat compression flanges stiffened by webs on both sides,  $k_{ls}$ , and on one side only,  $k_{lu}$ , can be determined with Eqs. (7) and (8), respectively.

$$k_{ls} = k_{ss} + k_{is}(k_{ff} - k_{ss}) \quad (7)$$

$$k_{lu} = k_{sfr} + k_{iu}(k_{ffr} - k_{sfr}) \quad (8)$$

where  $k_{ss} = 4$  and  $k_{ff} = 6.97$  are buckling coefficients for long plate simply supported on all sides and for long plate fixed on long sides and simply supported on short sides, respectively;  $k_{sfr} = 0.425$  and  $k_{ffr} = 1.277$  are buckling coefficients for long plate simply supported on one long side and both short sides and free on another long side and for long plate fixed on one longer side, free on another long side and simply supported on short sides, respectively;  $k_{is}$  and  $k_{iu}$  are interaction coefficients for flat stiffened and unstiffened deck flanges, respectively, determined using Eqs. (9) and (10).

$$k_{is} = 0.98 - 1.66 Y_{na}/h_d \quad (9)$$

$$k_{iu} = [271.28(Y_{na}/h_d) - 225.77(Y_{na}/h_d)^2 - 81.20]k_{tu} \quad (10)$$

$$k_{tu} = 1.04 + 12.54t - 288.28t^2 \quad (11)$$

Figure 19 shows that the proposed equations predicted buckling coefficients observed in the FE simulations reasonably well.

Based on the relationship between  $M_{u,FEA}/M_{u,DSM}$  and  $Y_{na}/h_d$  shown in Fig. 14a, the nominal moment capacity of deck with flat compression flanges governed by local buckling can be predicted using Eqs. (12)-(14).

$$M_{nl} = \begin{cases} M_y \text{ for } \lambda_l \leq (0.5 + \sqrt{0.25 - a})^{\frac{1}{2\alpha}} \\ \left[1 - a \left(\frac{M_{crl}}{M_y}\right)^\alpha\right] \left(\frac{M_{crl}}{M_y}\right)^\alpha M_y \text{ for } (0.5 + \sqrt{0.25 - a})^{\frac{1}{2\alpha}} < \lambda_l \leq 3.517 \end{cases} \quad (12)$$

$$a = \begin{cases} 0.16 - 0.004(Y_{na}/h_d)^{-3.94} & \text{for } 0.39 < Y_{na}/h_d \leq 0.64 \\ 0 & \text{for } 0.37 \leq Y_{na}/h_d \leq 0.39 \end{cases} \quad (13)$$

$$\alpha = \begin{cases} 1.53(Y_{na}/h_d)^{2.21} & \text{for } 0.39 < Y_{na}/h_d \leq 0.64 \\ 0.2 & \text{for } 0.37 \leq Y_{na}/h_d \leq 0.39 \end{cases} \quad (14)$$

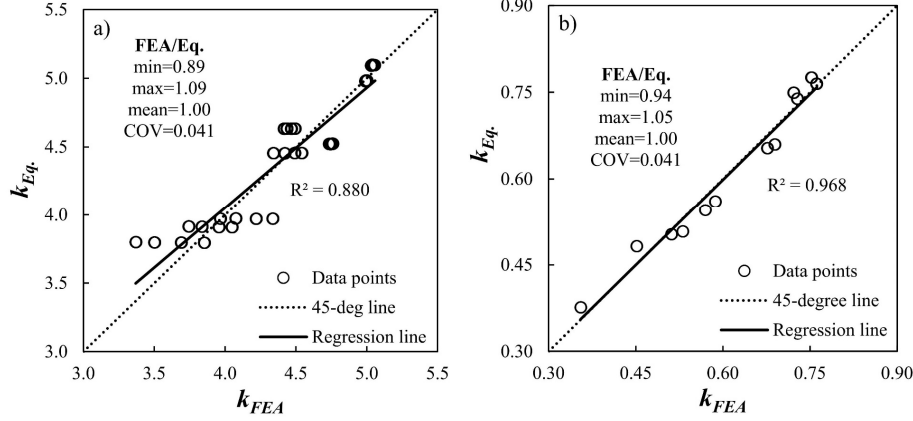


Figure 19: Comparisons of local buckling coefficients of deck with flat compression flanges predicted using proposed equations with those obtained from FE simulations for a) flanges stiffened by webs on both sides and b) flanges stiffened by webs on one side only

The nominal moment capacity of deck with flat compression flanges governed by distortional buckling can be predicted as follows:

$$M_{nd} = \begin{cases} M_y & \text{for } \lambda_d \leq 0.820 \\ \left[1 - 0.22 \left(\frac{M_{crl}}{M_y}\right)\right] \left(\frac{M_{crl}}{M_y}\right) M_y & \text{for } 0.820 < \lambda_d \leq 1.373 \end{cases} \quad (15)$$

Comparisons of the flexural resistances predicted by the proposed equations with those obtained from the FE simulations presented in Fig. 20 show that the developed equations can predict the strength of decks with flat compression flanges reasonably well.

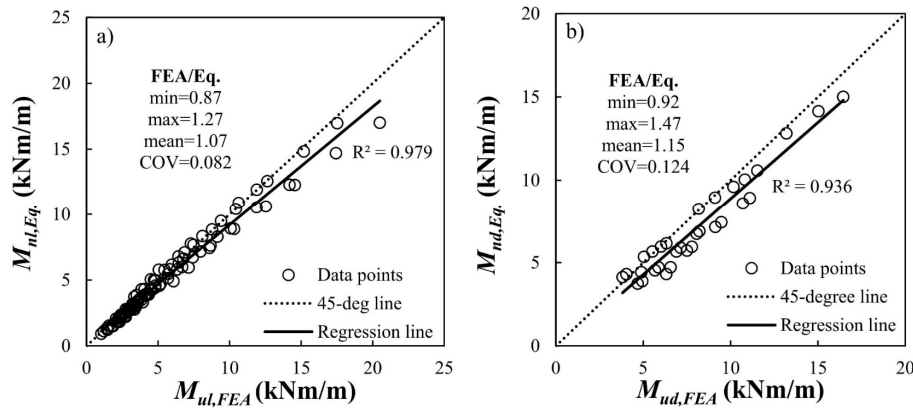


Figure 20: Comparisons of ultimate moments of deck with flat compression flanges predicted using proposed equations with those obtained from FE simulations for a) local and b) distortional buckling

According to Bulson (1970) and AISI S100-16, elastic distortional buckling load of plates with longitudinal intermediate stiffeners is a function of  $\gamma = 10.92I_{sp}/(b_o t^3)$  and  $\delta = A_s/(b_o t)$ , where  $I_{sp}$  is moment of inertia of stiffener about centerline of flat portion of plate,  $b_o$  is total flat width of stiffened plate, and  $A_s$  is gross area of stiffener. The elastic distortional buckling coefficients,  $k_d$ , for deck compression flanges with longitudinal intermediate stiffeners obtained from the FE simulations are plotted against  $\gamma$  in Fig. 21.

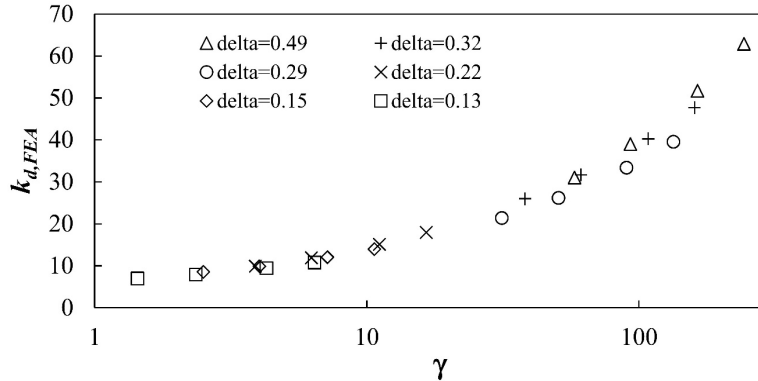


Figure 21: Effects of  $\gamma$  and  $\delta$  on distortional buckling coefficient

The relationship between  $k_d$ ,  $\gamma$ , and  $\delta$  shown in Fig. 21 can be described by the following equations obtained from a regression analysis of the FE simulation results:

$$k_d = a\gamma^\alpha \quad (16)$$

$$a = 6.96 - 5.65\delta \quad (17)$$

$$\alpha = 0.65\delta^{0.36} \quad (18)$$

Figure 22 shows a very good agreement of the distortional buckling moments predicted using Eqs. (16)-(18) with those obtained from the FE simulations.

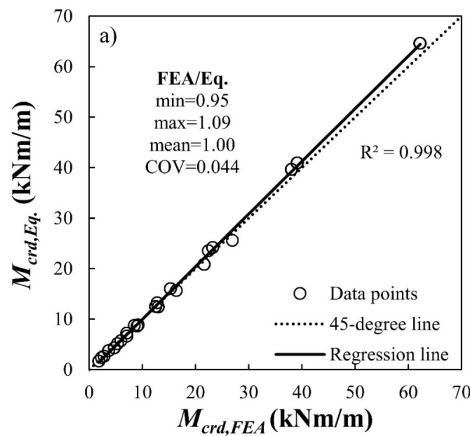


Figure 22: Comparison of distortional buckling moments predicted using proposed equations with those obtained from FE simulations for deck with longitudinal intermediate stiffeners in compression flanges

No design recommendations were developed for the flexural resistance of the deck with longitudinal intermediate stiffeners in compression flanges and for the deck with flat compression

flanges failing in distortional buckling because the current DSM provisions compared reasonably well with the FE simulation results and the data obtained in this study was insufficient for developing improved equations.

## 5. Conclusions

Elastic buckling and post-buckling strength of CFS deck in bending have been investigated using numerical methods. Numerical FE models were validated against published experimental results with good agreement observed, after which an extensive parametric study was carried out on trapezoidal deck profiles with different heights, thicknesses, and yield stresses commonly used in the US. Compression flanges of the studied deck profiles were either flat or had longitudinal intermediate stiffeners of different sizes. Different boundary conditions, presence of transverse ties, and different steel constitutive models were other parameters of the study. The different boundary conditions consisted of the deck supported by top flanges and loaded through bottom flanges and the deck supported by bottom flanges and loaded through top flanges.

The different boundary conditions of the deck resulted in a relatively small (0-4%) difference in the elastic buckling moments and in a significant (up to 26%) ultimate moment reduction in some profiles when the deck was loaded through top flanges and supported by bottom flanges. Transverse ties, which simulated deck side lap connections and prevented deck panels from spreading, resulted in an increase in the elastic buckling moments up to 9%. When the transverse ties were added to the models, the ultimate moment of the deck supported by top flanges and loaded through bottom flanges increased by 0-4%, whereas the ultimate moments of the deck supported by bottom flanges and loaded through top flanges increased by 6-18%. The different constitutive models of steel considered in the study—elastic-perfectly plastic, bilinear, and nonlinear—had relatively small effects on the ultimate moments of the deck models.

The elastic buckling coefficients for deck flat compression flanges obtained from the FE simulations depended on the relative depth of the deck compression zone,  $Y_{na}/h_d$ , and were considerably greater than the plate buckling coefficients for small  $Y_{na}/h_d$  ratios and slightly smaller than the plate buckling coefficients for large  $Y_{na}/h_d$  ratios. Deck profiles with flat compression flanges, especially non-symmetrical profiles with wider flanges in compression, failing in local buckling exhibited considerable post-buckling strength. DSM of AISI S100-16 provided overly conservative predictions of the flexural strengths for the non-symmetrical profiles with wider flanges in compression and reasonably good predictions of the flexural strength for similar symmetrical profiles. Therefore, the post-buckling strength of the decks with flat compression flanges is a function of not only the deck flange slenderness, but also the level of the deck non-symmetry, which can be expressed either by the ratio of the deck flange widths or by  $Y_{na}/h_d$ . EWM provided better predictions of the flexural strength for the deck with flat flanges failing in local buckling than DSM, but the flexural strengths of the deck failing in distortional buckling predicted by EWM were not conservative for profiles with large slenderness factors.

Local elastic buckling moments of decks with longitudinal intermediate stiffeners in compression flanges obtained from FE simulations showed good agreements with those predicted by the AISI S100-16 provisions. The distortional buckling moments predicted with the AISI S100-16 equations were smaller than the distortional buckling moments from the FE simulations. The DSM and EWM equations showed slight non-conservatism in predicting flexural strength of the deck

with flange stiffeners failing in local buckling. The DSM strength curve for distortional buckling showed a reasonably good agreement with the FE simulation results, except for a non-symmetrical deck with small stiffeners in wider compression flanges, which flexural strength was under-predicted by DSM. EWM provided less conservative predictions of the flexural strength for the deck failing in distortional buckling, especially for slender deck sections, than DSM. Decks with small slenderness considered in the study demonstrates considerable (up to 35%) inelastic reserve strength.

Design equations have been proposed for predicting local elastic buckling coefficients of deck with flat compression flanges and distortional buckling coefficients of deck with longitudinal intermediate stiffeners in compression flanges. Modifications of DSM for better predictions of the flexural strength of deck with flat compression flanges failing in local and distortional buckling have been also proposed. The proposed equations agreed well with the FE simulation results.

## References

- Schafer, B.W. (2019). "Advances in the Direct Strength Method of cold-formed steel design." *Thin-Walled Structures*, 140, 533-541.
- AISI S100-16. (2016). "North American Specification for the Design of Cold-formed Steel Structural Members." *American Iron and Steel Institute*, Washington, DC.
- AS/NZS 4600:2018. (2018). "Cold-formed steel structures." *Standards Australia. Standards New Zealand*.
- Schafer, B.W. (2008). "Review: The Direct Strength Method of cold-formed steel member design." *Journal of Constructional Steel Research*, 64, 766-778.
- Schafer, B.W., Peköz, T. (1998). "Direct Strength prediction of cold-formed steel members using numerical elastic buckling solutions." *Proceedings of Fourteenth International Specialty Conference on Cold-Formed Steel Structures*, St. Louis, MO, 69-76.
- Höglund, T. (1980). "Design of trapezoidal sheeting provided with stiffeners in the flanges and webs." *Swedish Council for Building Research D28*, Stockholm, Sweden.
- Bernard, E.S., Bridge, R.Q., Hancock, G.J. (1993). "Tests of profiled steel decks with V-stiffeners." *Journal of Structural Engineering*, 119(8), 2277-2293.
- Dudenbostel, R.K., Sputo, T. (2016). "Application of the Direct Strength Method to steel deck." *Proceedings of Wei-Wen Yu International Specialty Conference on Cold-Formed Steel Structures*, Baltimore, MD, 665-679.
- Raebel, C., Gwozdz, D. (2018). "Comparison of experimental and numerical results for flexural capacity of light-gage steel roof deck." *Proceedings of Wei-Wen Yu International Specialty Conference on Cold-Formed Steel Structures*, St. Louis, MO, 55-67.
- ANSYS Mechanical APDL, Release 19.2.
- Schafer, B.W., Li, Z., Moen, C.D. (2010). "Computational modeling of cold-formed steel." *Thin-Walled Structures*, 48, 752-762.
- Fauth, C. (2015). "Guidelines and recommendations for integrating specific profiled steels sheets in Eurocodes (GRISPE)." *D 3.3 Test report. Karlsruhe Institute of Technology (KIT)*, Karlsruhe, Germany. <http://www.grispeplus.eu/7-families-of-steel-profiles/perforated-and-holed-profiles/>
- EN 1993-1-3:2006. (2006). "Eurocode 3 - Design of steel structures - Part 1-3: General rules - Supplementary rules for cold-formed members and sheeting." *European Committee for Standardization*, Brussels, Belgium.
- Gardner, L., Yun, X. (2018). "Description of stress-strain curves for cold-formed steels." *Construction and Building Materials*, 189, 527-538.
- EN 1993-1-5:2006. (2006). Eurocode 3 - Design of steel structures - Part 1-5: Plated structural elements. European Committee for Standardization. Brussels, Belgium.
- Degtyarev, V.V. (2020). "Finite element modeling of cold-formed steel deck in bending." *Magazine of Civil Engineering*, 94(2).
- Bulson, P.S. (1970). "The stability of flat plates." *Chatto & Windus*, London.